



---

### **D3.1 | Read-out scheme**

**Author(s):** Zhuoran Geng, Ilari Maasilta

**Delivery date:** 13.2.2020

**Version:** 2.0

---



This project has received funding from the European Union's Horizon 2020 research and innovation programme under grant agreement No 800923.

Project Acronym:	SUPERTED
Project Full Title:	Thermoelectric detector based on superconductor-ferromagnet heterostructures
Call:	H2020-FETOPEN-2016-2017
Topic:	FETOPEN-01-2016-2017
Type of Action:	RIA
Grant Number:	800923
Project URL:	<a href="https://superted-project.eu/">https://superted-project.eu/</a>

Editor:	Ilari Maasilta, University of Jyväskylä
Deliverable nature:	Report (R)
Dissemination level:	Public (PU)
Contractual Delivery Date:	29.2.2020
Actual Delivery Date:	13.2.2020
Number of pages:	16
Keywords:	Bolometer, calorimeter, read-out, SQUID
Author(s):	Zhuoran Geng, University of Jyväskylä Ilari Maasilta, University of Jyväskylä
Contributor(s):	Tero Heikkilä, University of Jyväskylä Heli Lehtivuori, University of Jyväskylä Alessandro Monfardini, Institute Néel, CNRS Florence Lévy-Bertrand, Institute Néel, CNRS
External contributor(s):	

## Abstract

This Deliverable 3.1 ‘*Read-out scheme*’ is a summary of the project’s results for the design of the read-out circuit for thermoelectric bolometers and calorimeters of THz and X-ray radiation, respectively. The aim of Work Package 3 is to demonstrate and characterize FI/S based systems with antennas (THz, continuum) or heavy-metal absorbers (X-ray, single events) as detectors of electromagnetic radiation in two distinct frequency regimes, and to propose a readout scheme including multiplexing strategy for each type of application. The deliverable describes arguments why a current read-out with a Superconducting Quantum Interference Device (SQUID) amplifier is suitable for both bolometric and calorimetric operation of a superconductor-ferromagnet thermoelectric detector. A more detailed numerical analysis considering three practical SQUID read-out schemes is presented. In addition, two possible multiplexing schemes are envisioned.



# 1. Introduction

The main aim of Work Package 3 (WP 3) is to demonstrate and characterize FI/S based systems with antennas (THz, continuum) or heavy-metal absorbers (X-ray, single events) as detectors of electromagnetic radiation in two distinct frequency regimes, and to propose a readout scheme including multiplexing strategy for each type of application. If the goal of radiation detection is to detect small signals, the sensor itself typically cannot produce a large enough signal to be read out directly by standard digital electronics: amplification of the signal is required. For an electrical sensor, the simplest option is to read out either the voltage or the current of the output of the transducer. Typically, voltage read-out is better suited for high-impedance sensors, whereas low-impedance sensors work better with current read-out. In this case, the superconductor-ferromagnet thermoelectric detector (SFTED) is a tunnel junction, which from the read-out point of view is not clearly in the low or high impedance limit, so *a priori*, it is not obvious which type of read-out works the best. The purpose of this deliverable is to answer this question and, in particular, to study how the read-out amplifiers need to be designed to optimize the total performance of the detector + read-out. Initial part of this study is discussed in our recently submitted manuscript [1], where we studied the feasibility of a SQUID readout in both bolometric and calorimetric regimes.

## 2. Read-out scheme for bolometers

To compare the performance of different types of bolometers, the noise-equivalent power (NEP) is often quoted as a key benchmark, which is defined as the input radiation power in 1 Hz bandwidth required by the detector to generate a signal equal to its noise. A theoretical approach to estimate the NEP for SFTED has been proposed by Heikkilä *et. al.* in 2018 [2]. In the theoretical approach [2], NEP is derived based on the fluctuation-dissipation theorem and the thermal and electrical balance of the device within small signal regime. It includes the typical Johnson noise and thermodynamic fluctuation noise and especially a negative cross-noise term between the junction current and heat current fluctuations, due to the strong thermoelectric response, which is not usually considered in other types of detectors. In the same article, the thermoelectric figure of merit  $ZT$ , NEP, and thermal time constant  $\tau_{th}$  were evaluated at the low frequency limit in a reasonable parameter space. The calculated results show that the SFTED can reach similar or better NEP than transition edge sensor (TES) bolometers [3–5], on the order of  $10^{-19}W/\sqrt{Hz}$  at low temperatures with sub-millisecond effective thermal time constants ( $\tau_{eff} = \tau_{th}\sqrt{1 + ZT}$ ).

The contribution of the zero-frequency amplifier noise for both voltage and current read-out schemes has also been briefly estimated and discussed in that article. The initial conclusion was that due to the large (low-frequency) junction impedance, a good low temperature voltage amplifier, for example with voltage noise spectral density  $\sqrt{S_V} = 0.3 \text{ nV}/\sqrt{Hz}$  [6], has an added noise much lower than the intrinsic noise of the SFTED. In contrast, the noise contribution of a good current amplifier was estimated to be dominant at low temperature and thus limiting the NEP performance of SFTED.



## 2.1 Issues with voltage read-out

Several technical issues exist and limit the performance and implementation of the voltage read-out scheme for SFTED. For example, the cryogenic bipolar transistor amplifier mentioned above has a voltage noise of only  $0.3 \text{ nV}/\sqrt{\text{Hz}}$ , but its current noise ( $60 \text{ fA}/\sqrt{\text{Hz}}$ ) will dominate the amplifier noise when a sensor resistance  $R_S$  is larger than  $R_{opt} = \sqrt{S_V}/\sqrt{S_I} = 5 \text{ k}\Omega$ . With SFTED, especially for bolometric applications, smaller junction sizes are required to match the antenna impedance. Thus, the dynamic impedance of the tunnel junction during operation can be in the range of few tens  $M\Omega$  to more than  $G\Omega$ , leading to a much degraded amplifier performance.

For high impedance sensors, the junction field effect transistor (JFET) is typically considered as the preamplifier of choice. Although it has very low input voltage noise ( $\sim \text{nV}/\sqrt{\text{Hz}}$ ) and the optimal resistance can be matched with SFTED, its operating temperature and power dissipation severely limit the applications for cryogenic detectors. At cryogenic temperature, a good Si-based JFET has a dissipation power of several  $mW$  [7], and degraded performance due to the ‘freeze-out’ phenomenon [8], which forces the JFET to be operated at temperature higher than  $100 \text{ K}$  [9], far above the liquid helium and the cold sensor stage temperatures. As a result of these issues, the detector bandwidth and the maximum number of pixels are both limited by the large stray capacitance from long wiring distance and the total preamplifier dissipation. For many applications, in particular for multiplexing of large sensor arrays, these become practical issues.

Other types of FET-based voltage preamplifiers, although maybe suitable to be mounted at  $4 \text{ K}$  stage such as the state-of-art AlGaAs/GaAs heterojunction FET (cryoHEMT), still suffer from the issues such as rather large power consumption at low temperature ( $< 0.5 \text{ mW}$ ), increased  $1/f$  noise at low frequency, and large amplifier capacitance ( $\sim 100 \text{ pF}$ ) [10].

Based on these general difficulties with FET read-outs, we have decided to consider the SQUID based current read-out in much more detail, as discussed below.

## 2.2 SQUID based current read-out for bolometer

In contrast to FETs, the Superconducting Quantum Interference Device (SQUID) based read-out scheme has several advantages. First, SQUIDs operate naturally at cryogenic temperatures and have low dissipation. The first SQUID stage can therefore be mounted close to the SFTED at the base temperature of the refrigerator, to minimize electronic interference and microphonic noise [11]. DC SQUIDs and its RT feedback electronics can operate typically with a bandwidth of  $\sim 10 - 20 \text{ MHz}$ , which means that the SQUID itself does not limit the response time of a bolometer. The impedance, in particular the capacitance of the tunnel junction has a negligible influence on the noise performance of the SQUID. Finally, several well-developed multiplexing schemes for SQUID read-out for large arrays have already been developed and have been fielded successfully [12–14].

However, a current read-out for SFTED is not as straightforward as with low-impedance TES detectors ( $R \sim 1 \text{ m}\Omega - 1 \Omega$ ). Because of the larger junction dynamic resistance, the current signal and



noise of the SFTED is usually very low ( $\sim fA/\sqrt{Hz}$ ) at low temperatures. In conventional SQUID read-out setups, (for TESes for example), the SQUIDs used have input current noise around  $pA/\sqrt{Hz}$ , which is thus expected to be too high for SFTED purposes.

### 2.2.1 Flux transformer coupled SQUID

To match the SQUID read-out better with the SFTED, we propose to use a superconducting flux transformer at the front end of the input coil of the SQUID itself. This reduces the input referred current noise. The concept scheme is shown in Figure 1

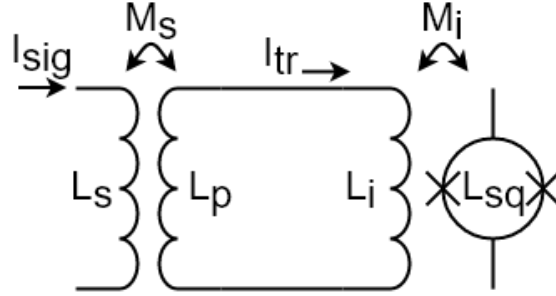


Figure 1: SQUID with a flux transformer at its input.

Due to the conservation of flux inside the transformer coil, we have:

$$\begin{cases} L_p I_{tr} + L_i I_{tr} = M_s I_{sig} + M_i I_{sq} \\ \Phi_{SQ} = L_{SQ} I_{SQ} = I_{tr} M_i \end{cases}, \quad (1)$$

where the self-inductances ( $L$ ), mutual inductances ( $M$ ) and currents ( $I$ ) of the circuit are defined in Fig. 1. The total mutual inductance will be obtained as:

$$M_T = \frac{M_s M_i}{L_p + L_i (1 - k_i^2)}, \quad (2)$$

with  $k_i$  the SQUID coupling factor which depends largely on the transformer geometry.

In the following section, we will computationally estimate the performance of an SFTED as a bolometer with SQUID current read-out with three different flux transformer setups based on already implemented SQUIDs and transformers.

Table 1: SQUID read-out setups comparison.

	Magnicon SQUID C6XXL116	VTT transformer+ Magnicon SQUID	Jena SQUID
Signal coil inductance $L_s$	1.8 $\mu H$	39 mH	9.5 mH
Winding ratio $n_s$	40:1	1284:2	48:1
Flux noise $\sqrt{S_\phi}$	0.25 $\mu\phi_0/\sqrt{Hz}$ @0.3 K	0.25 $\mu\phi_0/\sqrt{Hz}$ @0.3 K	1 $\mu\phi_0/\sqrt{Hz}$ @4 K
Total coupling factor $k_{tot}$	0.74	0.14	0.51
Current noise $\sqrt{S_I}$	$\sim 60 fA/\sqrt{Hz}$ @0.3 K	$\sim 2 fA/\sqrt{Hz}$ @0.3 K	$\sim 3 fA/\sqrt{Hz}$ @4 K



The main parameters of these SQUID setups are listed in Table 1. The Magnicon transformer coupled SQUID setup was first developed and experimentally demonstrated by Drung *et al.* [15] in PTB Germany, and then commercialized by Magnicon GmbH. The second setup we propose is a combination of an extremely large winding ratio flux transformer, which was developed and experimentally demonstrated by J. Luomahaara *et al.* [16] at VTT Finland, with another Magnicon SQUID. And the third Jena SQUID setup was developed and measured by V. Zakosarenko *et al.* [17] in Jena Germany.

In the next section we use these values to estimate the SFTED performance in various conditions.

### 2.2.2 Performance of SFTED bolometer with SQUID read-out

Here, we numerically estimate the performance of the SFTED with the above mentioned three SQUID setup options. The detector parameters that were chosen for the comparisons are shown in Table 2. The parameter values are realistic estimates based on what is known about the properties of existing EuS tunnel barrier devices.

**Table 2: Bolometer parameters**

Al energy gap	$\Delta(0) = 200 \text{ meV}$
Broadening parameter	$1 \times 10^{-4} \Delta(0)$
Exchange field	$0.6 \Delta(0)$
Al thickness	$10 \text{ nm}$
Junction area	$1 \times 10 \mu\text{m}^2$
Barrier material	EuS
Specific transparency	$100 \text{ k}\Omega\mu\text{m}^2$
Polarization	0.9
Parasitic capacitance	$1 \text{ nF}$

The finite frequency total NEP of SFTED with a current read-out can be calculated to read:

$$NEP_{tot}^2(\omega) = a_0 \omega^0 + a_1 \omega^2 + a_2 \omega^4 + a_3 \omega^6, \quad (3)$$

where

$$a_0 = NEP_{TED}^2(0) + \frac{S_{amp}}{\alpha^2} (G_{th}^{tot})^2 T^2,$$

$$a_1 = NEP_{TED}^2(0) \tau_{eff}^2 + \frac{S_{amp}}{\alpha^2} [(G_{th}^{tot})^2 T^2 \tau_{th}^2 - 2LC(G_{th}^{tot})^2 T^2 + G^2 L^2 (G_{th}^{tot})^2 T^2 - 2GTG_{th}^{tot} L^2 \alpha^2 - 2G_{th}^{tot} LT \tau_{th} \alpha^2 + L^2 \alpha^4],$$

$$a_2 = \frac{S_{amp}}{\alpha^2} [L^2 C^2 (G_{th}^{tot})^2 T^2 - 2LC \tau_{th}^2 (G_{th}^{tot})^2 T^2 + 2CTG_{th}^{tot} \tau_{th} L^2 \alpha^2 + G^2 L^2 \tau_{th}^2 (G_{th}^{tot})^2 T^2],$$



$$a_3 = \frac{S_{amp}}{\alpha^2} C^2 L^2 \tau_{th}^2 (G_{th}^{tot})^2 T^2,$$

where the  $NEP_{TED}(0)$  is the detector zero-frequency NEP,  $S_{amp}$  is the noise current spectral density of the (SQUID) preamplifier, and other symbols follow the definitions of reference [2].

Figure 2(a) shows the total NEPs (detector + read-out) of SFTED at 1 kHz, with the three different SQUID setups as a function of bath temperature. By comparing them with the detector intrinsic NEP (blue solid line), we observe that the Magnicon SQUID read-out (red dash-dotted line) will dominate the total NEP due to its relatively large current noise. In contrast, for the VTT (red dash line) or Jena (red dotted line) SQUID read-out at operating temperatures  $> 0.2$  K, the detector is still the main source of noise. This can be seen more directly from the current noise spectral density comparison shown in Figure 2(b). It should be noted here that typical SQUID read-outs used currently for most operating TESes have current noise  $> 1 pA/\sqrt{Hz}$ , many orders of magnitude above the detector noise. For operating temperatures below  $\sim 0.2$  K, the total NEP is saturated by the amplifier noise, but is of the order of  $10^{-19} W/\sqrt{Hz}$ , which still meets the bolometer design requirements of the SFTED (Targeted NEP  $1 - 10 \times 10^{-18} W/\sqrt{Hz}$ ).

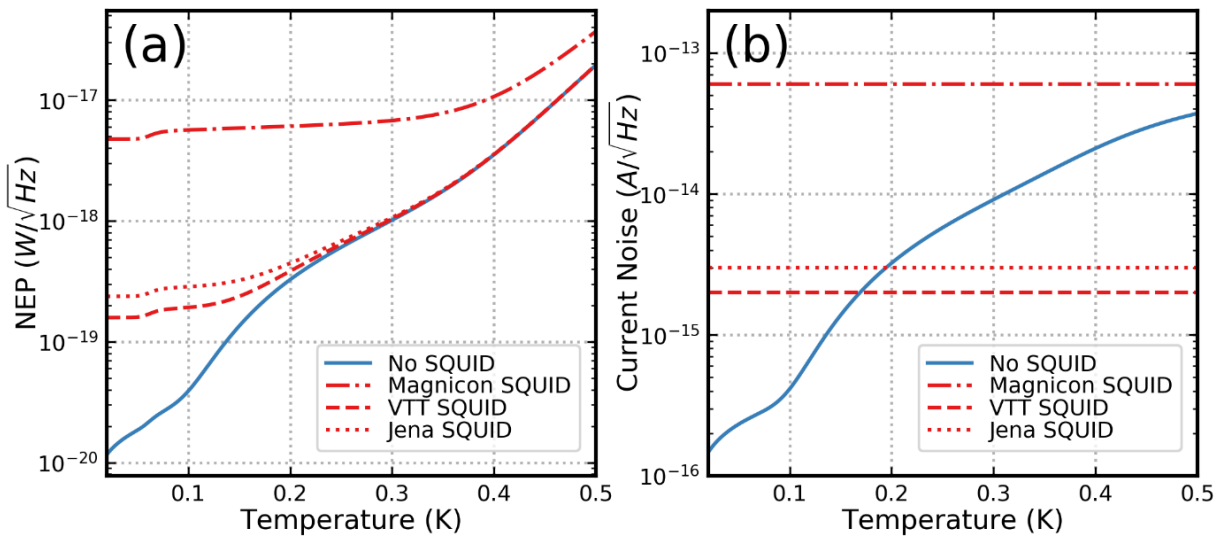
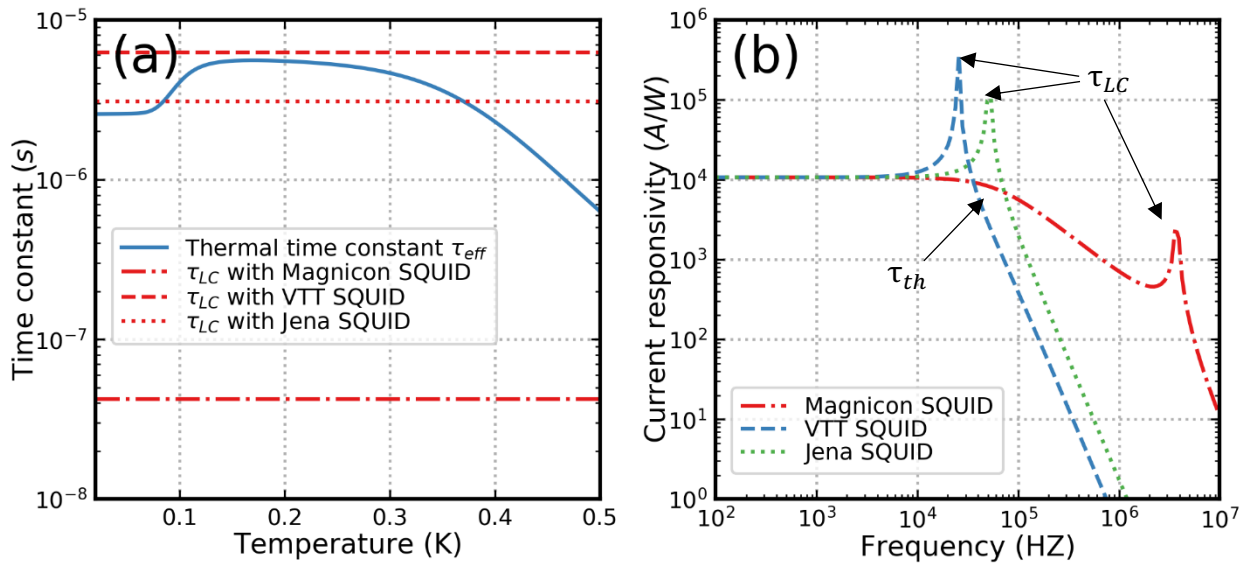


Figure 2: (a) Total NEP with different SQUIDs, (b) comparison of the SQUID and detector noise

The time constants of the above detector and read-out setups are shown in Figure 3(a). The thermal time constant of the detector is independent of the read-out, and is shown as the blue solid line. Without considering extra damping or any additional cut-offs from the higher stage electronics, the electrical time constant is determined mainly by the inductance of the front-end signal coil. The VTT transformer (dashed line) has the largest inductance in the signal coil, which limits its bandwidth to  $\sim 10$  kHz and completely dominates the effective time constant. The speed with the Magnicon SQUID setup (red dash-dotted line), however, is determined by the detector thermal time constant. In this case, the benefit of obtaining a larger bandwidth by using a smaller signal coil is diminished by the thermal cut-off of the signal responsivity, as shown in Figure 3(b) in frequency domain at temperature of 0.1 K: the responsivity diminishes when the frequency becomes larger than  $1/\tau_{th}$ . For



the Jena SQUID (dotted line), although the thermal time constant dominates at 0.1–0.3 K, to damp the LC resonance, the bandwidth is still determined by the electrical time constant, being of the order of  $\sim 10$  kHz.



**Figure 3(a) Comparison of the electrical time constants of the SQUIDs to the thermal time constant (b) Frequency dependent responsivity with different SQUIDs**

Another drawback of using a large ratio flux transformer besides the increased electric time constant is the slow signal tracking speed of the flux lock loop (FLL) of the read-out amplifier. For a typical SQUID slew rate of  $1 \phi_0/\mu\text{s}$ , the VTT or Jena setup has a signal tracking speed of  $< 10$  nA/ $\mu\text{s}$ , which means that the SQUID amplifier loses its locking on any input signal that changes faster. By comparison, the SQUID used for TES application normally has a tracking speed of  $10 \mu\text{A}/\mu\text{s}$ , allowing larger and faster input pulses to be measured.



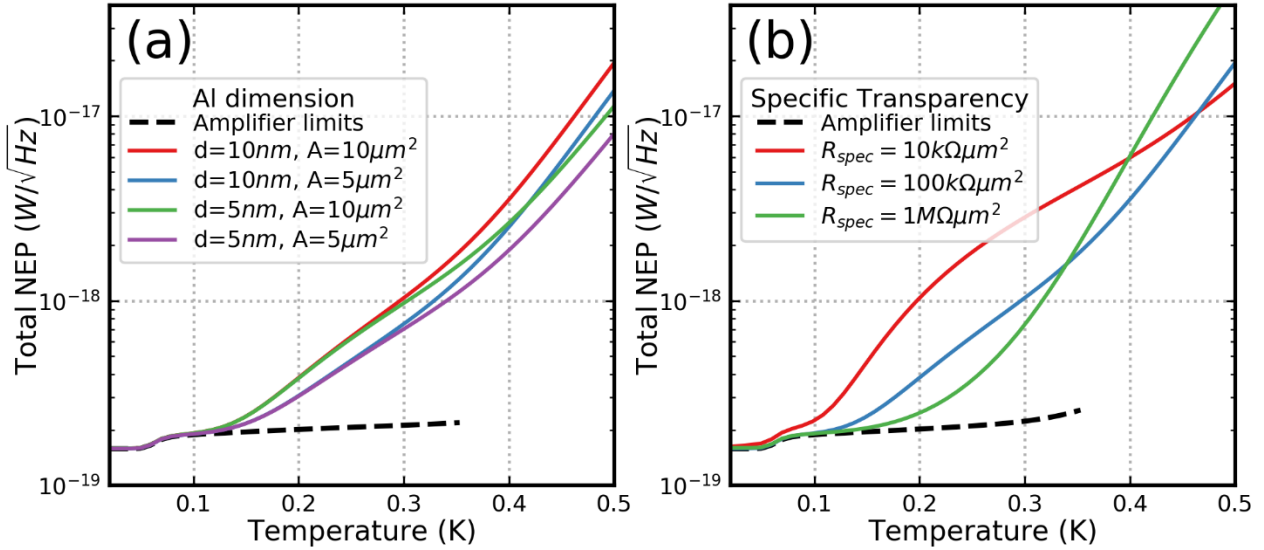


Figure 4 Crossover from amplifier limited NEP (dashed line) to detector limited NEP at high  $T$

As explained above, with the SQUID read-out, the NEP of the SFTED bolometer is limited by the amplifier at the lowest temperatures  $< 0.2$  K. The crossover between the amplifier limited and the intrinsic detector limited NEP does not move much with changes in the junction area or barrier thickness (Figure 4(a)), but is pushed to slightly higher operating temperatures by decreasing the specific transparency of the tunnel barrier, i.e., decreasing its area (Figure 4(b)).

### 3. Read-out scheme for X-ray calorimeters

For X-ray calorimeters, the energy resolution  $\Delta E$  (*rms*) is the main figure of merit. Under the small signal assumption, an optimal filter can be applied to the signal pulse, and the energy resolution can be estimated by [18]:

$$\Delta E = \left( \int_0^\infty \frac{4df}{NEP^2} \right)^{-\frac{1}{2}}. \quad (4)$$

To achieve a good energy resolution, a large bandwidth is crucial for the detector. However, unlike a bolometer, an X-ray calorimeter requires an absorber which has more matter and preferably heavier elements to efficiently absorb the incident energy. This leads to a several orders of magnitude larger detector overall volume, and correspondingly, a much longer thermal time constant.

#### 3.1 Performance of SFTED calorimeter with SQUID read-out

Table 3: EuS Calorimeter

Al energy gap	$\Delta(0) = 200 \text{ meV}$
Broadening parameter	$1 \times 10^{-4} \Delta(0)$



Exchange field	$0.6\Delta(0)$
Absorber volume (Al)	$1 \times 10^4 \mu\text{m}^3$
Junction area	$1 \times 10^4 \mu\text{m}^2$
Barrier material	EuS
Specific transparency	$100 \text{ k}\Omega\mu\text{m}^2$
Polarization	0.9
Parasitic capacitance	$1 \text{ nF}$

Here, we estimate the performance of a much larger SFTED calorimeter (parameters shown in Table 3) with the same three different SQUID read-out setups as before. The resulting energy resolutions and time constants are shown in in Figure 5. With all three read-outs, SFTED is predicted to reach sub-eV energy resolution below  $150 \text{ mK}$ , potentially outperform the best of TESes [19] and MMCs [20]. Particularly at an operating temperature below  $300 \text{ mK}$ , the energy resolution of SFTED with VTT or Jena SQUID read-out is completely dominated by the detector, but even the Magnicon SQUID could be used to advance the state-of-the-art. Note that the thermal time constant of the detector is now longer than the SQUID time constants at low temperature (Figure 5(b)), which limits the bandwidth and count rate of the detector, but the same issue exists with all other bolometric calorimeter technologies.

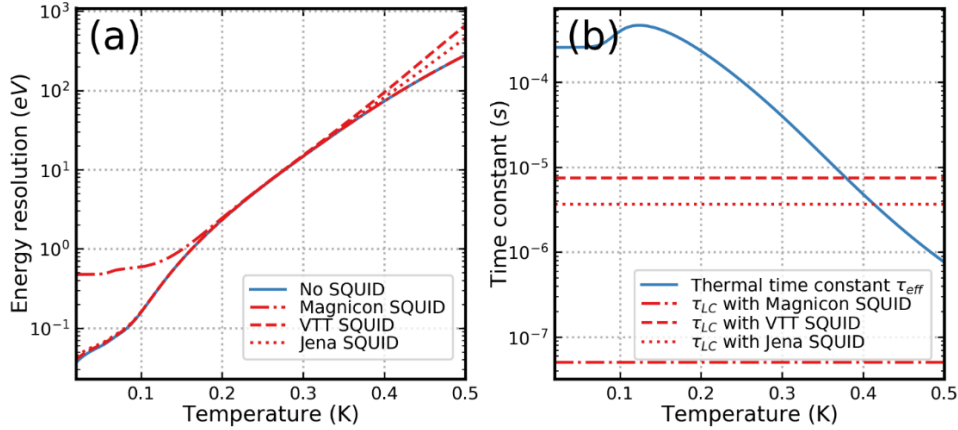


**Figure 5(a) The energy resolution and (b) time constants of a SFTED X-ray calorimeter with the different SQUID options.**

At low temperatures, the heat conductance through the tunnel junction is much higher than that for the electron-phonon relaxation. In that case, we can roughly estimate the thermal time constant by:

$$\tau_{th} = F \cdot \frac{V}{A} R_{spec}, \quad (5)$$

where  $F$  is a material dependent prefactor,  $V$  is the volume of the absorber,  $A$  is the area of the tunnel junction, and  $R_{spec}$  is the specific transparency of the tunnel barrier. Therefore, in the same



geometric design, the detector bandwidth can be increased by engineering the tunnel barrier of the junction to be more transparent.

To reach to a time constant of  $\mu\text{s}$ , the EuS tunnel barrier should have a specific transparency of  $\sim 1\text{ k}\Omega\mu\text{m}^2$  as shown in Figure 6(b). With such a detector, the Magnicon SQUID read-out will outperform other two setups due to its larger bandwidth, and has an energy resolution  $< 2\text{ eV}$  up to  $200\text{ mK}$  (red dash-dotted line in Figure 6(a)).

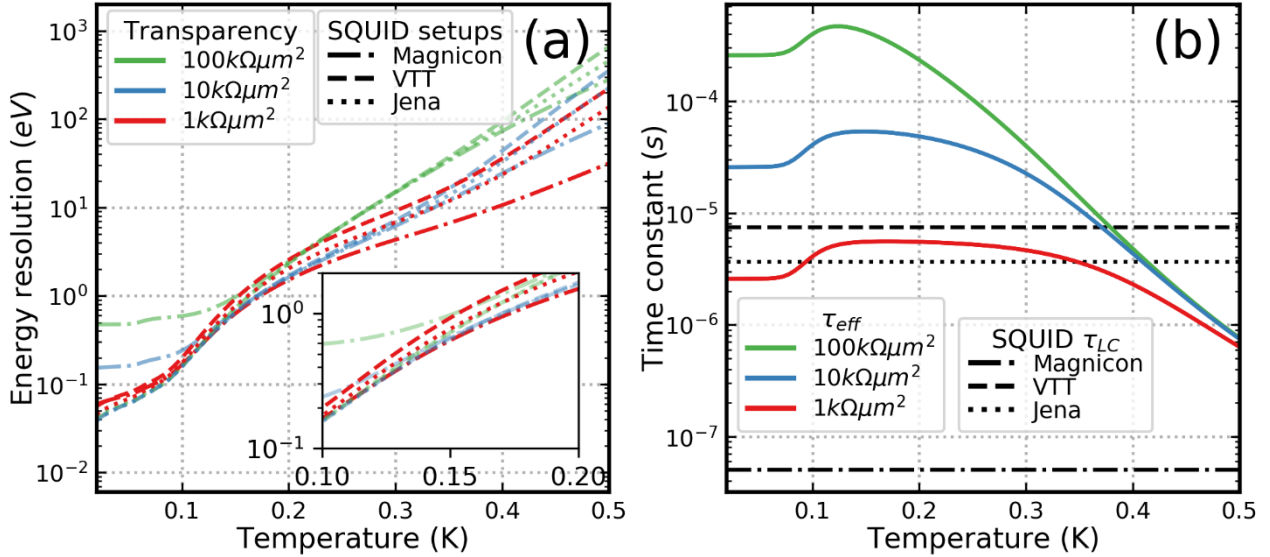


**Figure 6 (a) Energy resolution and (b) time constant vs T for different SQUIDs and junction transparencies, EuS barrier device.**

Alternatively, a more transparent AlOx barrier can also be used for the tunnel junction, combined with a ferromagnetic electrode for spin filtering (Fe, Co, etc.). AlOx barriers can easily have specific transparencies  $\sim 0.1 - 10\text{ k}\Omega\mu\text{m}^2$ . In Figure 7, the characteristics for a SFTED with AlOx barrier with transparency  $1\text{ k}\Omega\mu\text{m}^2$  (polarization of 0.3 and an exchange field of  $0.3\Delta$  [1]), are calculated with the different SQUIDs. With the Magnicon SQUID read-out, a detector dominated  $\sim\text{ eV}$  total energy resolution can be expected at operating temperature  $150 - 200\text{ mK}$ , while a high bandwidth with a time constant of  $\sim\mu\text{s}$  is retained as shown in Figure 7.



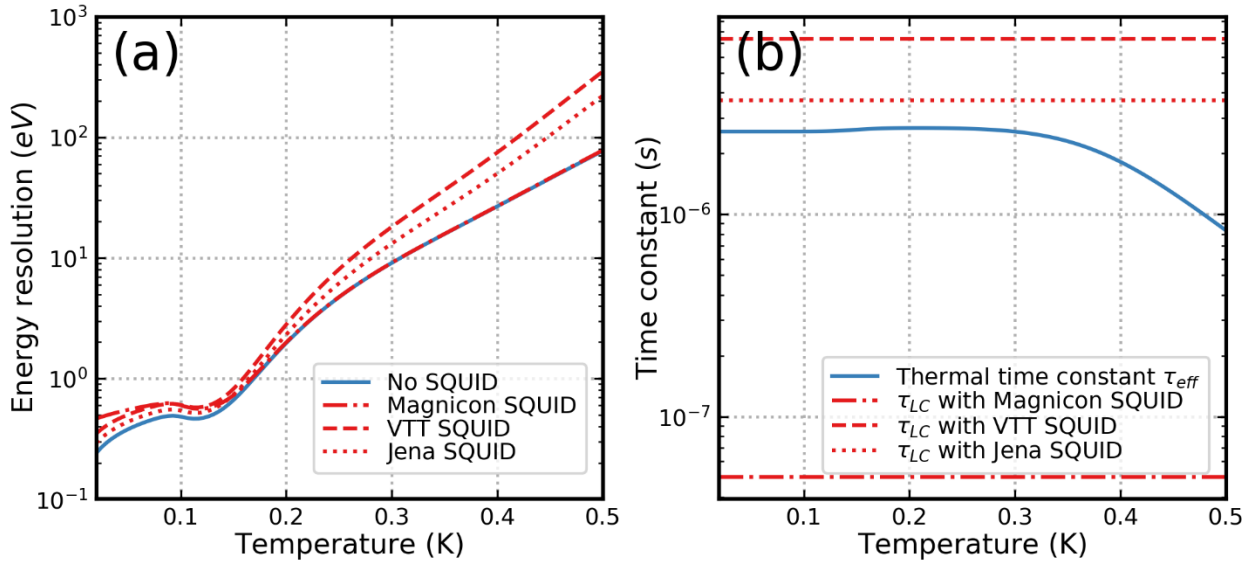


Figure 7 Energy resolution and (b) time constant vs T for different SQUIDs and junction transparencies, AlOx barrier device.

Thus, the Magnicon SQUID current read-out is preferable with a transparent detector junction barrier. It provides a good combined energy resolution, meeting our requirement ( $< 2$  eV), a large bandwidth that is comparable with high count rate TESes, and thus has potential for larger array multiplexing, and a signal tracking speed (slew rate) of  $\sim 0.3 \mu\text{A}/\mu\text{s}$  for operational stability.

### 3.2 Possible multiplexing schemes

To further improve the collection efficiency, count rate and to add imaging capabilities, large arrays of sensors are preferred over the single pixel implementation. Multiplexing is almost always crucial for the development of large arrays, since it gives thermal and financial benefits over the full read-out circuitry for each pixel. Several well-developed SQUID multiplexing schemes for large arrays have been experimentally demonstrated [13,14,21], which can also be implemented for the SFTED microcalorimeter application without the need of separate sensor biasing circuitry.

A possible time-division multiplexing (TDM) scheme is shown in Figure 8. Each sensor has a dedicated flux transformer and first stage SQUID read-out (SQ1). Each row of SQUIDs is biased in series with a timed sequence, and the output signals are collected by the column-wise summing coils and measured by the secondary SQUIDs (SQ2). The  $M$  column by  $N$  row TDM read-out can be multiplexed by  $M + N$  signal lines instead of  $M \times N$  needed without multiplexing.



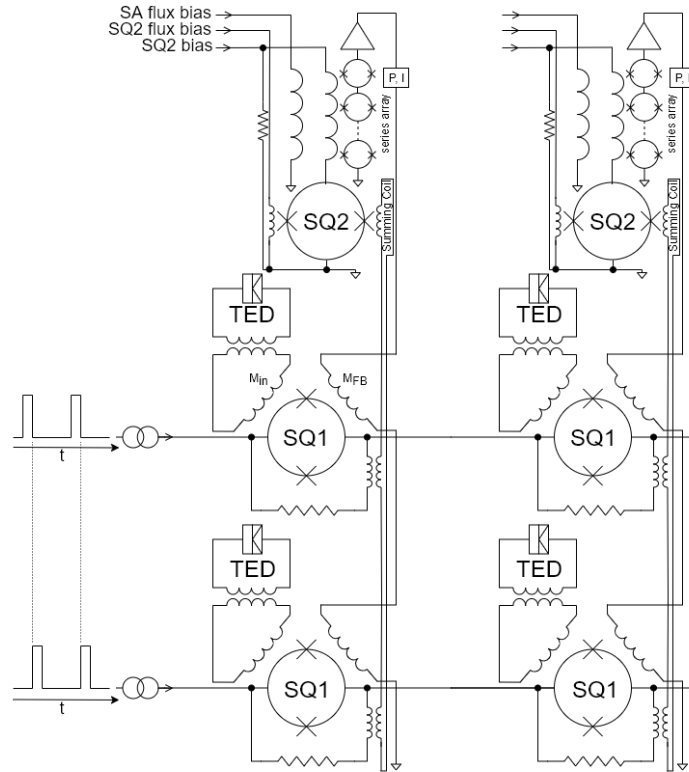


**Figure 8 Possible scenario for time-division multiplexing (TDM) of SFTEDs**

For a SQUID setup similar to the Magnicon read-out, the system has a more than ten times faster electrical response than the thermal time constant (Fig. 7 (b)), which determines the relaxation time of the X-ray pulse signal. Therefore, high switching rate ( $1/\delta t_s$ ) and sampling rate ( $1/N\delta t_s$ ) are possible for the multiplexer to sample the signal with high fidelity.

The simplicity and maturity of TDM makes it a good candidate for a potential multiplexing scheme for SFTED. It also allows one to run each pixel in a non-multiplexed mode for individual pixel characterization and debugging. The main drawback of TDM is that the effective SQUID current noise scales as  $\sqrt{N}$  due to the aliasing of the high switching bandwidth, eventually limiting the pixel performance [12].

An alternative scheme is code-division multiplexing (CDM), in which the output signal of each pixel is orthogonally modulated by Walsh codes (highly auto-correlated but zero cross-correlated) [22] functions, measured sequentially in each row, and separated at last by a matrix operation. A possible flux summation ( $\phi$ -CDM) implementation is shown in Figure 9. In this setup, the  $N$  input coils for each sensor are connected in series but with different polarizations based on Walsh codes, and are coupled to all  $N$  flux transformers and first stage SQUIDs (SQ1). These SQUIDs are switched on in a timed sequence, and the output signals are collected by a summing coil and measured by the secondary SQUID (SQ2).





project. At the moment, we have in mind a plan to combine a transformer similar to that was demonstrated at VTT [16] with a Magnicon SQUID. VTT has already been consulted, and they still have the mask designs available. Details on compatibility and integration with Magnicon SQUID and how the fabrication could be organized need further discussion. We will also initiate a discussion with Magnicon/PTB on whether they could tailor something along those lines for the project.

### 4.3 Kinetic Inductance Detector based current readout for bolometer

A promising approach that will be investigated in Grenoble is based on the non-linearity of the kinetic inductance against the current that is circulating in a superconducting thin film. By placing such a current-dependent inductance in a microwave resonator, the small currents generated by the thermoelectric effect can be measured through their effect on the resonator's frequency. In order to achieve the wanted non-linearity, disordered superconductor materials, like AlOx or others, will be employed. The first demonstration of this concept has been achieved by M. R. Vissers and collaborators in 2015 [23]. The advantage of this approach lies in the large multiplexing factor that is potentially achievable, and the use of existing KID readout electronics in CNRS. Moreover, the wiring in the cryostat will be greatly simplified.

## 5. Conclusions

We have done a detailed analysis of whether SQUID preamplifiers can be used to read-out SFTED detectors, both as bolometers and calorimeters. It indicates that both types of detectors can be read-out by practical SQUIDs in combination with a flux transformer. The SQUID types considered for the bolometer are not fully matched to a EuS barrier SFTED at the lowest temperatures, but, the degradation of performance is not significant in the sense that we estimate that the targeted NEP values can be surpassed by an order of magnitude, to reach  $\sim 10^{-19} \text{ W}/\sqrt{\text{Hz}}$ . This gives a margin of tolerance for unanticipated experimental factors that might degrade the performance further.

For X-ray calorimeters, even the simplest considered SQUID read-out choice (commercially available Magnicon SQUID) can be used effectively for both EuS and AlOx barrier devices. In fact, it is preferred over the more complex setups, because it gives the best overall performance due to its much faster speed. In particular, there would be a large advantage for multiplexing.

The principles outlined here must also be partially used to guide the detector fabrication to ensure that the detector performance is not degraded too much by the read-out. A parameter wishlist from the read-out point of view will be maintained on the project wiki pages.

## Bibliography

- [1] Z. Geng, A. P. Helenius, T. T. Heikkilä, and I. J. Maasilta, ArXiv:1908.04097 (2019).
- [2] T. T. Heikkilä, R. Ojajarvi, I. J. Maasilta, E. Strambini, F. Giazotto, and F. S. Bergeret, Phys. Rev. Appl. **10**, 034053 (2018).
- [3] B. S. Karasik and R. Cantor, Appl. Phys. Lett. **98**, 193503 (2011).



- [4] A. D. Beyer, M. Kenyon, P. M. Echternach, B. Bumble, M. C. Runyan, T. Chui, C. M. Bradford, W. A. Holmes, and J. J. Bock, in *Millimeter, Submillimeter, Far-Infrared Detect. Instrum. Astron. VI*, edited by W. S. Holland (2012), p. 84520G.
- [5] T. Suzuki, P. Khosropanah, M. L. Ridder, R. A. Hijmering, J. R. Gao, H. Akamatsu, L. Gottardi, J. van der Kuur, and B. D. Jackson, *J. Low Temp. Phys.* **184**, 52 (2016).
- [6] N. Beev and M. Kiviranta, *Cryogenics (Guildf)*. **57**, 129 (2013).
- [7] D. Yvon, V. Sushkov, R. Bernard, J. L. Bret, B. Cahan, O. Cloue, O. Maillard, B. Mazeau, J. P. Passerieux, B. Paul, and C. Veyssiere, *Nucl. Instruments Methods Phys. Res. Sect. A Accel. Spectrometers, Detect. Assoc. Equip.* **481**, 306 (2002).
- [8] R. T. Goldberg, M. D. Jhabvala, R. K. Kirschman, S. Wang, G.-H. Gwo, and J. A. Lipa, in *Proc. Symp. Low Temp. Electron. High Temp. Supercond.* (1995), pp. 428–439.
- [9] L. He, J. Hao, Z. Deng, F. Liu, Y. Liu, Y. Li, Q. Yue, and J. Cai, in *J. Phys. Conf. Ser.* (Institute of Physics Publishing, 2019).
- [10] Y. Jin, Q. Dong, U. Gennser, L. Couraud, A. Cavanna, and C. Ulysse, in *2016 13th IEEE Int. Conf. Solid-State Integr. Circuit Technol. ICSICT 2016 - Proc.* (Institute of Electrical and Electronics Engineers Inc., 2016), pp. 342–345.
- [11] M. Frank, C. A. Mears, S. E. Labov, F. Azgui, M. A. Lindeman, L. J. Hiller, H. Netel, and A. Barfknecht, *Nucl. Instruments Methods Phys. Res. Sect. A Accel. Spectrometers, Detect. Assoc. Equip.* **370**, 41 (1996).
- [12] J. N. Ullom and D. A. Bennett, *Supercond. Sci. Technol.* **28**, 084003 (2015).
- [13] M. Kiviranta, H. Seppä, J. van der Kuur, and P. de Korte, in (2003), pp. 295–300.
- [14] K. D. Irwin and K. W. Lehnert, *Appl. Phys. Lett.* **85**, 2107 (2004).
- [15] D. Drung, C. Aßmann, J. Beyer, A. Kirste, M. Peters, F. Ruede, and T. Schurig, in *IEEE Trans. Appl. Supercond.* (2007), pp. 699–704.
- [16] J. Luomahaara, M. Kiviranta, and J. Hassel, *Supercond. Sci. Technol.* **25**, 035006 (2012).
- [17] V. Zakosarenko, M. Schmelz, R. Stolz, T. Schönau, L. Fritzsche, S. Anders, and H. G. Meyer, *Supercond. Sci. Technol.* **25**, 095041 (2012).
- [18] K. D. Irwin and G. C. Hilton, in *Cryog. Part. Detect.* (2005).
- [19] S. J. Smith, J. S. Adams, M. E. Eckart, C. N. Bailey, S. R. Bandler, J. A. Chervenak, M. E. Eckart, F. M. Finkbeiner, R. L. Kelley, C. A. Kilbourne, F. S. Porter, and J. E. Sadleir, in *J. Low Temp. Phys.* (2012), pp. 168–175.
- [20] C. Pies, S. Schäfer, S. Heuser, S. Kempf, A. Pabinger, J. P. Porst, P. Ranitsch, N. Foerster, D. Hengstler, A. Kampkötter, T. Wolf, L. Gastaldo, A. Fleischmann, and C. Enss, in *J. Low Temp. Phys.* (2012), pp. 269–279.
- [21] J. A. Chervenak, K. D. Irwin, E. N. Grossman, J. M. Martinis, C. D. Reintsema, and M. E. Huber, *Appl. Phys. Lett.* **74**, 4043 (1999).
- [22] J. L. Walsh, *Am. J. Math.* **45**, 5 (1923).
- [23] M. R. Vissers et al, *Appl. Phys. Lett.* **107**, 062601 (2015).

